D32

EVALUATION OF ALGORITHMS FOR GEOLOGICAL THERMAL-INERTIA MAPPING

S. H. Miller and Kenneth Watson

U.S. Geological Survey, Denver, Colorado

ABSTRACT

The errors incurred in producing a thermal-inertia map are of three general types: measurement, analysis, and model simplification. To emphasize the geophysical relevance of these errors, we express them in terms of uncertainty in thermal inertia and compare these uncertainties with the thermal-inertia values of geologic materials. Thus the applications and practical limitations of the technique are illustrated.

All errors are calculated using the parameter values appropriate to a site at the Raft River, Id. Although these error values serve to illustrate the magnitudes that can be expected from the three general types of errors, extrapolation to other sites should be done using parameter values particular to the area.

Measurement errors introduced by multispectral scanning systems commonly range from a noise-equivalent-temperature difference (NEΔT) of 0.1K for aircraft systems to 1K for satellite systems. The resulting uncertainties in thermal inertia range from 15 TIU (thermal-inertia unit)* to 150 TIU.

Three surface temperature algorithms were evaluated: linear Fourier series, finite difference, and Laplace transform. In terms of resulting errors in thermal inertia, the Laplace-transform method is the most accurate (260 TIU), the forward finite-difference method is intermediate (300 TIU), and the linear Fourier series method the least accurate (460 TIU). However, the two more exact methods require more computer time, and both lack the ability of the Fourier-series algorithm to illustrate the physical significance of individual terms. By comparing the errors with the range of thermal inertias of geologic materials, it is possible to select the most cost/effective algorithm for a particular application.

Model simplification errors result from three sources: transient effects, topography, and surface coating effects. For example, flux of 35 watts/m^2 (equivalent to a water evaporation rate of 1.2 mm/day) would produce a thermal-inertia error of about 200 TIU. If no topographic corrections are made, a 10° southwestern slope causes an error in thermal inertia of about 350 TIU. A hematite surface coating one centimeter thick on a rock will produce an error of approximately 200 TIU, whereas a one-millimeter layer thickness will have a negligible effect (25 TIU).

The total system errors in thermal inertia are placed in geologic context by noting the separation in thermal-inertia values for various geologic materials. For example, the thermal-inertia separation between limestones and dolomites is typically 1200 TIU. The error analysis technique indicates that thermal-inertia discrimination should be possible between black shale and gabbro (separation of approximately 450 TIU); discrimination between these two materials was not possible using Landsat spectral-reflectance data.

Errors in thermal inertia can be translated into errors in bulk density and moisture content. Thermal-inertia mapping from aircraft (NEΔT = 0.1K) has an accuracy of about 1% in bulk density or equivalently, a sensitivity of 0.3% in water content. From satellite (NEΔT = 1K) these accuracies are 9% and 3% respectively.

A practical evaluation of the error analysis is demonstrated for aircraft data acquired at Raft River, Id. We cannot discriminate the tuff from the alluvium, having a lower thermal inertia, and the lava, having a higher thermal

* TIU = 1 watt $\cdot$ $sec^{\frac{1}{2}}/m^2/K$

inertia, without a topographic correction, but we can discriminate the lava flows from the alluvium.

1. INTRODUCTION

Thermal-inertia mapping is a recently developed technique that allows discrimination among geologic materials [1], [2], [3], [4], [5], [6]. The purpose of this paper is to discuss the types and magnitudes of errors encountered in applying this technique and to express these errors in a geologically meaningful way. The errors are of three major types: measurement errors, analysis errors, and model simplification and assumption errors. The major focus of this paper is to develop a procedure to select an algorithm which is appropriate to the geologic application and which minimizes computer time.

In addition to presenting the mathematical basis for the three algorithms, we provide a numerical evaluation with respect to an exact solution. Estimates of the errors due to measurement and model simplification are combined with the analysis errors, and all errors are expressed as uncertainties in thermal inertia. These combined errors are compared to the thermal-inertia values determined for some selected geologic situations. As an illustration of the analysis technique, the Fourier-series algorithm is applied to the construction of a thermal-inertia map of an area in the Raft River, Id.

2. MATHEMATICAL BASIS

Thermal inertia is a physical property of geologic materials, and its value can be determined by measurements of the diurnal variation of surface temperature and the albedo of the surface. A physical model for the surface temperature variation is therefore required.

We assume one-dimensional, periodic heating of a uniform half space of constant thermal properties. The ground temperature obeys the diffusion equation:

$$\kappa \frac{\partial^2 v(x,t)}{\partial x^2} = \frac{\partial v(x,t)}{\partial t} \qquad (1)$$

where $v(x,t)$ is the ground temperature at a distance x below the surface and a time t, and κ is the thermal diffusivity.

To solve this equation for the surface temperature, we require a form of the solution appropriate to the diffusion equation and the boundary condition, which assumes conservation of energy over the diurnal cycle. Before looking at possible forms of the solution, we need to investigate the boundary condition.

If we assume a heat-balance condition exists at the surface, then the incoming heat fluxes--the incident solar radiation (I), the sky radiation (S), and the geothermal heat flux (Q)--must balance the outgoing fluxes--the convective flux (C), the evaporative flux (E), and the ground reradiation flux (R). The resulting expression of the heat flux at the surface is:

$$-K \frac{\partial v(x,t)}{\partial x}\bigg|_{x=0} = I + S + Q - C - E - R \qquad (2)$$

where K is the conductivity of the material. The convective and evaporative fluxes are included in equation 2 for completeness; however those terms will be handled only qualitatively in this paper.

The parameter of interest, the surface temperature, is present in equation 2 in the heat-conduction term (the left hand side of equation 2) and in the ground-reradiation term (R). Equation 2 is rewritten to display the surface temperature:

$$-K \left. \frac{\partial v(x,t)}{\partial x} \right|_{x=0} = -\varepsilon\sigma\, v(0,t)^4 + a(t) + Q \qquad (3)$$

where ε is the mean emissivity of the ground, σ is the Stefan-Boltzmann constant, a(t) is a term combining the time-dependent solar flux and sky radiation flux and thus includes the surface albedo and emissivity, and Q is the geothermal heat flux. This expression must be satisfied for any equational form of v(x,t) chosen for the solution to the diffusion equation. The nonlinear form of this boundary condition prevents a direct analytical solution of the diffusion equation. An exact numerical solution can be calculated [7]; however, the complexity, the difficulty of illustrating the physical significance of terms, and the computer costs all provide incentive for investigating less exact algorithms.

One method of handling the nonlinear boundary condition is to linearize it and to express the solution to this condition in an exact form as an infinite Fourier series. The linearization is achieved by performing a Taylor-series expansion of the surface temperature around the sky temperature and discarding quadratic and higher order terms. This solution has been discussed in detail by Watson [1], and the form of this solution is:

$$v(0,t) = T_{sky} + \frac{Q}{s} + (1-A)\, S_o C \cdot \sum_{n=0} \frac{\cos(n\omega t - \varepsilon_n - \delta_n)}{\sqrt{(s+r\sqrt{n})^2 + (r\sqrt{n})^2}} \qquad (4)$$

where

$$s = 4\varepsilon\sigma T_{sky}^{\,3}$$

$$r = P\sqrt{\frac{\pi}{\tau}}$$

$$\tau = \frac{2\pi}{\omega}$$

$$\delta_n = \tan^{-1}\left(\frac{r\sqrt{n}}{s + r\sqrt{n}}\right)$$

and T_{sky} is the sky temperature, A is the ground albedo, C is an effective atmospheric-transmission factor, S_o is the solar constant, Q is the geothermal heat flux, A_n and ε_n are the amplitude and phase of the nth harmonic of the insolation, and P is the thermal inertia.

Another method of solving the diffusion equation is to use the exact, nonlinear boundary condition and to apply a finite-difference iterative technique [9]. This solution assumes the form:

$$V_{m+1,n} - 2 \cdot V_{m,n} + V_{m-1,n} = \frac{(\Delta x)^2}{\Delta t \cdot \kappa} (V_{m,n+1} - V_{m,n}) \qquad (5)$$

where $V_{m,n}$ is the ground temperature at a time, $n\Delta t$, and distance from the surface, $m\Delta x$; Δx and Δt are small increments in distance and time; and κ is the diffusivity.

The forward finite-difference method requires an initial solution and propagates this solution forward in time. To insure continuity at the boundary, the heat-balance boundary condition must be satisfied. The boundary condition for the forward finite-difference solution is expressed as:

$$V_{0,n+1} = V_{1,n+1} + \frac{\Delta x}{K} f\left\{V_{0,n+1}, (n+1)\ \Delta t\right\} \qquad (6)$$

where K is the conductivity and f is the flux (eq. 2).

Numerical stability and convergence put constraints on the size of the time and distance increments. To insure these errors do not grow, the stability condition

$$\kappa \cdot \frac{\Delta x}{(\Delta t)^2} \leq 0.5 \qquad (7)$$

must be met [9].

The third method of solving the diffusion equation is to use the nonlinear boundary condition and to apply Jaeger's method of Laplace transforms [7]. This method has the advantage that it directly yields the surface temperature without requiring an estimate of the temperatures at depths. However, the solution also must be iterated due to its nonlinear form:

$$F_n = \frac{P}{\sqrt{\pi\tau}} \cdot \sum_{s=1}^{m} v_s \, \phi_{n-s+1} \qquad n=1,2,\ldots, m \qquad (8)$$

where F_n is the average flux into the ground in the nth time interval; P is the thermal inertia; τ is the period of the heating flux; v_s is the average surface temperature in the sth time interval; and the ϕ's are a set of numerical coefficients determined solely by m, the total number of intervals in τ. A detailed description of this method can be found in Jaeger [7] for the periodic heating of a half space, and the method was extended by Watson [8] to the heating of a layer over a half space.

3. ANALYSIS ERRORS

The previous section presents the mathematical basis for the three algorithms used to compute the diurnal surface temperatures (eq. 4, 5, 8). In this section, we numerically compare the errors by expressing the temperature differences as equivalent differences in thermal inertia. The difficulty in perceiving the physical significance of terms and the amount of computer time required for each algorithm are also discussed.

The evaluation of the algorithms in terms of uncertainties in thermal inertia is performed in two steps. The first is to compare the three algorithms with each other by approximating the incident solar flux as a sinusoidal half wave. The second step is to compare the most exact algorithm--the Laplace transform--with an exact theoretical solution--a pure sinusoid flux. This establishes the relationships of the three methods to the exact solution. The resulting errors in thermal inertia for each of the algorithms compared to the exact solution are:

Laplace-transform Algorithm	260 TIU
Finite-difference Algorithm	300 TIU
Fourier-series Algorithm	460 TIU

Table 1 gives the list of parameter values used to make the above comparison.

The relative ordering of the algorithms with respect to accuracy is as expected: the Laplace-transform algorithm, which is an implicit relationship between surface temperature and surface flux, is the most accurate; next the finite-difference solution; and lastly the Fourier-series algorithm, which linearizes the radiation-transfer terms. The magnitude of the errors can be made more geologically meaningful by noting that soils typically have thermal inertias in the range of 500 to 2000 TIU and that rocks typically have a range of thermal inertias of 2000 to 4000 TIU. (A more detailed discussion of the thermal inertias of geologic materials is presented in the discrimination of geologic materials section.)

An important consideration in the cost/effectiveness of thermal-inertia mapping is the computer time required to solve the various algorithms. In the

above comparison, the finite-difference and the Laplace-transform algorithms were both iterated until a day/night surface-temperature difference of less than one degree was achieved between iterations. The Fourier-series algorithm requires the computation of a series summation but requires no iteration. The Laplace-transform algorithm requires twice as many iterations as does the finite-difference algorithm. The actual number of iterations depends upon the complexity of the boundary condition and the accuracy desired. Thus the relative ranking of the algorithms in increasing order of required computer time is the Fourier series, the finite difference, and the Laplace transform.

Another consideration in performing thermal-inertia mapping is the need to be able to see the relationship between various parameters and surface temperature. From a knowledge of such relationships, the importance of various parameters on the calculation of thermal inertia is seen. Only the Fourier-series solution (eq. 4) allows this awareness. For example, the form of the solution suggests a mean temperature level that is modulated by the amplitude and phase of the harmonic term. We can recognize that changes in the geothermal heat flux or changes in the emissivity will produce a shift in the diurnal temperature curves; changes in the albedo will result in changes in both the mean level and the amplitude of the diurnal temperature. Thus a day/night temperature difference, which is a measure of this amplitude, does not contain, to first order, the effects of sky temperature, geothermal flux, or the zero-order term of the insolation. A recognition of these and similar relationships led to Watson [1] developing methods for both thermal inertia-mapping and geothermal heat-flux mapping.

Table 2 summarizes the results of this section.

4. TOTAL SYSTEM ERRORS

Measurement errors introduced by the multispectral scanning system impose a fundamental instrumental limitation on thermal-inertia mapping. These errors are the result of a combination of factors, including the noise limit of the detector, amplifiers, tape recorder, and, for a satellite system, down-link telemetry. These errors are commonly expressed as noise-equivalent-temperature differences (NEΔT). For an aircraft system, a typical value for a state-of-the art system is 0.1K. A 1K NEΔT is representative of a satellite system such as Nimbus III and IV; the HCMM (Heat Capacity Mapping Mission) satellite system may have a slightly lower NEΔT. These values of uncertainty in temperature convert to approximately 15 TIU for the aircraft and 150 TIU for a satellite. These resultant errors are in addition to the errors introduced by the mapping technique and represent a fundamental limitation inherent to the technique.

An error common to mapping data with both aircraft and satellite is that produced in the process of registering images acquired at different times. Because of changes in the vehicle path and scanner orientation (pitch, yaw, and roll), a point on the ground will not have the same image coordinates at two acquisition times. Daytime images acquired at the same time are automatically registered with each other and are geometrically identical. These "matched" images are called image-pairs. The registration is performed by selecting reference features on a master image-pair and subsequently identifying those features on the remaining "distorted" image-pairs and on the nightime thermal images. Reference features identified on both the master reflectance image and the master thermal image must be identified on the "distorted" nighttime thermal images but may be located on either the reflectance or the thermal image of "distorted" daytime image-pairs. The choice depends upon whether the appearance of the feature is governed by topography, thermal inertia, or reflectance. These reference features are then used as input to a triangular interpolation algorithm.

The errors due to misregistration are of two types. The first is a misregistration of an image-pair to the master image-pair. This misregistration results in an association of incorrect albedos and/or incorrect temperature-difference computation--both of which result in an inaccurate calculation of thermal inertia.

The second type of error is a misregistration of a calculated thermal inertia to a topographic map. This error is an inaccuracy in the assignment of a thermal inertia to a particular geographical point. We have not estimated the magnitude of these errors; however, we have qualitatively examined them.

Misregistration of either type results from one of two conditions: the spatial frequency of the misregistration is higher than the spacing of the reference features or the image features are not discernible enough to select suitable reference points. The first of these conditions--the rapidly varying scene--is correctable by choosing more frequent reference points, and the resulting errors in thermal inertia can be minimized. The additional points do impose a significantly higher computer time. The second condition--low scene contrast--is common especially in nighttime imagery. In such situations the best estimate of the location of a reference feature on an image-pair is made by scaling the distance from other identifiable features. In this case, the resulting registration may be geometrically inaccurate but numerically equivalent due to the resulting low contrast image, which will not exhibit much variation in temperature and/or reflectance values. Thus, these errors produced in computing or assigning thermal inertia are small. The edge effects that may be produced by identifying features by scaling can be reduced by spatial filtering.

In addition to the measurement errors, another important source of error in thermal-inertia mapping results from simplifications introduced by a particular model. These simplifications include the exclusion of transient fluxes, topography, and/or surface-coating effects.

Transient effects are those resulting from such conditions as cloudiness, windiness, or ground moisture. Effects of this type can be viewed as a flux perturbation on the periodic solution [11]. To illustrate this situation, we consider a heat-flux perturbation of 35 watts/m^2. The magnitude of this perturbation is equal to 2.5% of the solar constant, or an equivalent change in sky temperature of 10°K, or the effect of an evaporation rate of 1.4×10^{-8} m/sec (1.2 mm/day). The transient-effect calculation was made by varying the duration of the perturbation and noting the resulting change in surface temperature at a later time. A graph expressing the resulting errors in thermal inertia is presented in figure 1. The maximum error introduced by this perturbing flux is approximately 200 TIU.

Correctable topographic effects require an assumption as to the scattering law for the sloping surface and the need to neglect reradiation between adjacent surfaces. We shall assume that the surfaces are Lambert reflectors, and thus the local solar flux is proportional to the cosine of the angle between the surface normal and the solar radiation. In that case, an east or west slope to the surface causes a phase shift in the diurnal temperature curves, and a north or south slope to the surface produces a change in amplitude of the diurnal curves. A surface oriented in any other direction produces a combination of phase shift and amplitude changes. Both changes result in erroneous day/night temperature differences. Similarly, slope and surface orientation affect the reflectivity and can cause erroneous determinations of albedo. Both temperature and albedo errors contribute to an incorrect determination of thermal inertia. The magnitude of this error (using the Raft River parameter values) for a 10° slope facing southwest is approximately 350 TIU with the maximum error in thermal inertia occurring for a southwestern facing surface (figure 2).

Surface coatings change both the surface reflectivity and the diurnal temperature; hence they affect the apparent thermal inertia of geologic materials. We examined the thermal effect of a hematite coating over a half space, having the average thermal inertia of igneous rocks. Figure 3 shows the implied change in equivalent thermal inertia for various thicknesses of this layer [8]. For example a hematite layer of 10 millimeters will produce a change in thermal inertia of approximately 200 TIU. If the layer thickness is less than 1 millimeter, the coating is transparent in terms of thermal-inertia mapping but will be observable as an albedo difference.

Of the three simplification effects described, only the topography correction is at a stage of development to be incorporated into the thermal-inertia mapping. The local variations in the surface staining, vegetation cover, and surface roughness occur at a scale which precludes detailed modeling because that would require detailed knowledge of these effects at every point in the test site. We consider these types of effects occurring at a local scale irreducible for any practical use of remote-sensing techniques. Similarly, topographic effects in localized areas due to departure from Lambert emission, reradiation between adjacent surfaces, or shadowing effects are also probably in the same category.

5. DISCRIMINATION OF GEOLOGIC MATERIALS

In the previous sections, the types and magnitudes of errors encountered in performing thermal-inertia mapping were discussed. Now these errors are placed in geologic context and thereby provide criteria for evaluating the entire procedure. Thus the selection of modeling algorithm and data-collection procedure can be examined in the light of a particular geologic situation.

As an illustration, assume that we wish to discriminate between limestone and dolomite from a satellite in a study site that is relatively flat and whose outcrops have iron-oxide stains of approximately one-millimeter thickness.

Error Sources	Error Magnitude
satellite measurement	150 TIU
topographic effects	0 TIU
typical surface-coating effects	25 TIU
typical transient effects	100 TIU
	275 TIU

These measurement and model simplification errors are now combined with the analysis errors. The total system errors for each algorithm are:

Algorithm	Approximate Total Error
Fourier series	750 TIU
Finite difference	600 TIU
Laplace transform	550 TIU

We now know that we cannot discriminate between geologic materials having a thermal-inertia difference of less than 750 TIU using the Fourier-series or of less than 550 TIU using the Laplace-transform algorithm.

Figure 4 shows thermal-inertia histograms of various sedimentary rocks [12, 13]. From the histograms, we can determine that a typical thermal inertia for limestones is 2200 TIU and for dolomites is 3500 TIU; thus the separation is greater than the least accurate of the algorithms. Since any of the three analysis algorithms can be used, the selection of the algorithm will be determined by the cost/effectiveness criteria and the Fourier series would be selected.

In the hypothetical case, if we wish to discriminate between sandstones and dolomites, which typically have a thermal inertia separation of 550 TIU, we must select the Laplace-transform algorithm.

Table 3 shows typical thermal-inertia values for a range of igneous rocks. The separation between a fine-grained felsic rock (rhyolite) and a coarse-grained felsic rock (granite) is only 200 TIU; the separation between rhyolite and a coarse-grained mafic rock (gabbro) is approximately 400 TIU. Discrimination of a fine-grained felsic rock from a coarse-grained felsic rock can be achieved with the Laplace-transform technique, using many iterations and shortening the time interval. Discrimination of a fine-grained felsic rock from a coarse-grained mafic rock can be achieved with either the finite-difference algorithm or the Laplace-transform algorithm, depending first upon the measurement and model errors and second upon the cost/effectiveness.

In the analysis of Landsat data, discrimination between black shale and gabbro was not possible using spectral-reflectance data [2]. The thermal inertia separation of these two materials is approximately 450 TIU (Table 4), [9, 13] and the magnitude of the separation indicates that discrimination by thermal inertia is practical even by satellite. Discrimination among basalt, andesite, argillite, and black chert was also reported to be not possible by Landsat. Table 4 shows that thermal-inertia discrimination should be possible between black shale and gabbro, between basalt/andesite and black chert, and between argillite and black chert. Discrimination among argillite, basalt, and andesite does not appear possible.

Thermal inertia of soils is dependent primarily on bulk density and moisture content. Figure five shows that there is a rough linear relationship between thermal inertia and density for dry materials. The addition of moisture to dry soil results in a rapid increase in thermal inertia. For example, dry sand has a thermal inertia of 590 TIU, and wet sand (8% moisture) has a thermal inertia of 1020 TIU. Thus, for sand, the thermal-inertia mapping from aircraft ($NE\Delta T$ = 0.1K) has an accuracy of about 1% in bulk density, or equivalently a sensitivity of 0.3% in water content. From satellite ($NE\Delta T$ = 1K) these accuracies are 9% and 3% respectively.

6. RAFT RIVER ILLUSTRATION

The method of analyzing errors in terms of uncertainties in thermal inertia was then applied to an analysis of a thermal-inertia map constructed of an area of the Raft River, Id. Reflectance and thermal data were acquired at five different times in the diurnal cycle from July 24 to July 31, 1974. Figure six is the thermal image acquired near solar noon (July 31); figure seven is the thermal image acquired near solar midnight (July 31). These two images were used to form the temperature-difference image. Figure eight is the daytime reflectance image used to form the thermal-inertia map.

Geometrically registered albedo and day/night temperature-difference images were formed according to the procedure outlined in the section on total system errors. A relative thermal-inertia image (figure 9) was then constructed from the images by forming the ratio of albedo to day/night temperature difference. The scale on the side of the image that relates the gray scale to absolute thermal-inertia values was determined from the Fourier-series algorithm using a sky temperature of 245°K and a cloud cover factor of 0.13. The sky temperature and cloud cover factor were determined using a least-squares model fit to all the repetitive thermal-scanner data for the site. In the formation of this image, no correction for topography was made.

From the above information, the total measurement and analysis errors are compiled as follows:

Errors	Magnitude
Fourier-series algorithm	460 TIU
Aircraft measurement	15 TIU

Three geologic materials have been discriminated on the thermal-inertia image [10]: lava flows, tuffs, and alluvium (figure 9). Histograms were constructed of the thermal-inertia values of these materials from the map. The lava flows have a thermal inertia of 2010 $\pm$ 250 TIU; the tuffs have a thermal inertia of 1470 $\pm$ 210 TIU; and the alluvium has a thermal inertia of 1090 $\pm$ 80 TIU. From a topographic map, the alluvium was determined to be on a flat surface; the tuff area has a slope of 7.9° and an azimuth (measured counterclockwise) of 225°; and the lava flows have a slope of 10° and an azimuth of 198°. Thus the error in thermal inertia due to topography is 0 TIU for alluvium, -95 TIU for tuffs, and +110 TIU for the lava flows. We therefore determined that we cannot discriminate the tuff from the alluvium and the lava without a topographic correction, but we can discriminate the lava flows from the alluvium.

7. SUMMARY

The utility of thermal-infrared surveys to discriminate geologic materials based on differences in their thermal properties has been recognized by previous investigators. The error analysis technique presented here provides the means to evaluate the validity and reliability of such discrimination. This technique also provides criteria for selecting the most cost/effective algorithm for a particular geologic application. In addition, it can be applied to determine the fundamental accuracy required, and thus whether aircraft or satellite (for example, HCMM) data would be appropriate. A parallel analysis technique could be developed for geothermal heat-flux mapping. Such a technique could express the various errors in terms of the minimum detectable geothermal heat flux.

Additional improvements in the mapping can be provided by incorporating a topographic correction into the model. One way of accomplishing this is to incorporate digital topographic data in a look-up table [6]. Another method would be to assume a reflection law and compute the topographic correction using three reflectance images. Additional refinements would include the addition of a diffuse illumination term in the insolation factor and a more detailed treatment of areal transient effects. In our treatment, the sky radiation and solar-transmission factor were assumed constant and were determined by a least-squares fit to the actual image data. A least-squares fitting including harmonic terms could be added to represent more accurately the actual areal transient effects.

This study--even with its assumptions and simplifications on the model--should provide a useful comparison of the errors encountered in thermal-inertia mapping. Most importantly, all the uncertainties in the mapping technique are described in the context of discriminating geologic materials.

8. REFERENCES

[1] Watson, Kenneth, 1975, Geologic applications of thermal infrared images: Proc. IEEE, v. 63, no. 1, p. 128-137.

[2] Watson, Kenneth, Rowan, L. C., and Offield, T. W., 1971, Application of thermal modeling in the geologic interpretation of IR images: Proc. 7th Internatl. Symp. on Remote Sensing of Environment, v. 3, p. 2017-2041.

[3] Rowan,L. C., Offield, T. W., Watson, Kenneth, Cannon, P. J., and Watson, R. D., 1970, Thermal infrared investigations, Arbuckle Mountains, Oklahoma: Geol. Soc. Amer. Bull., v. 81, p. 3549-3562.

[4] Pohn, H. A., 1976, A comparison of Landsat images and Nimbus thermal-inertia mapping of Oman: Jour. Res. U.S. Geol. Survey, v. 4, no. 6, p. 661-665.

[5] Pohn, H. A., Offield, T. W., and Watson, Kenneth, 1975, Thermal-inertia mapping from satellite--discrimination of geologic units in Oman: Jour. Res. U.S. Geol. Survey, v. 2, no. 2, p. 147-158.

[6] Kahle, A. B., 1977, A simple thermal model of the earth's surface for geologic mapping by remote sensing: Jour. Geophys. Res., v. 82, no. 11, p. 1673-1680.

[7] Jaeger, J. C., 1953a, Pulsed surface heating of a semi-infinite solid: Quart. Appl. Math., v. 11, p. 132-137.

[8] Watson, Kenneth, 1973, Periodic heating of a layer over a semi-infinite solid: Jour. Geophys. Res., v. 78, no. 26, p. 5904-5910.

[9] Carslaw, H. S., and Jaeger, J. C., 1959, Conduction of heat in solids: 2d ed., New York, Oxford Univ. Press.

[10] Kline, R. J., 1977, Discrimination of geologic materials by thermal-inertia mapping within the Raft River test site: Master's thesis, Colorado School of Mines (in press).

[11] Watson, Kenneth, 1971, A thermal model for analysis of infrared images: NASA 3d Annual Earth Resources Program Review, Houston, Texas, v. 1, sec. 13, p. 1-16.

[12] Robie, R. A., and Waldbaum, D. R., 1968, Thermodynamic properties of minerals and related substances at 298.15°K (25.0°C) and one atmosphere (1.013 bars) pressure and at higher temperatures, U.S. Geol.

[13] Clark, S. P., Jr., Ed., 1966, Handbook of physical constants, revised edition, Geol. Soc. Amer. Memoir, v. 97, 587 p.

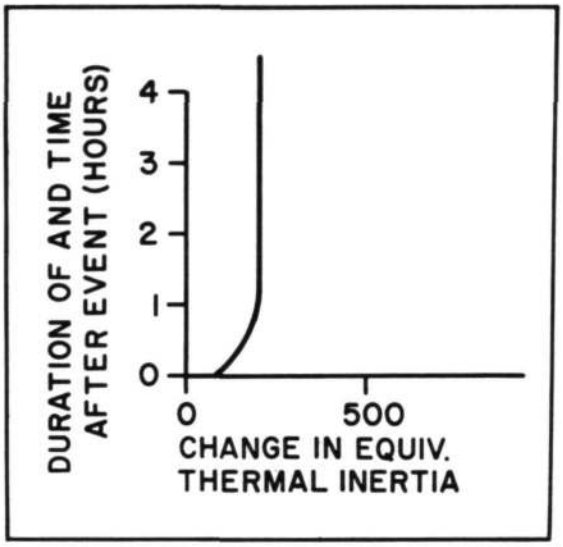

Figure 1.--Change in equivalent thermal inertia for a 35 watt/m^2 perturbing flux.

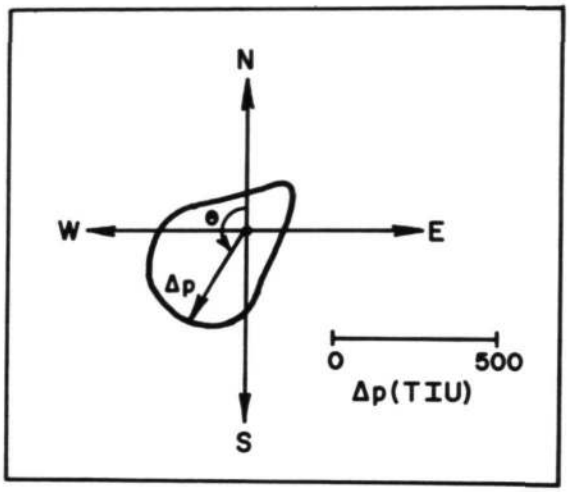

Figure 2.--Polar plot of change in equivalent thermal inertia for a 10° slope for variable azimuth angles (θ).

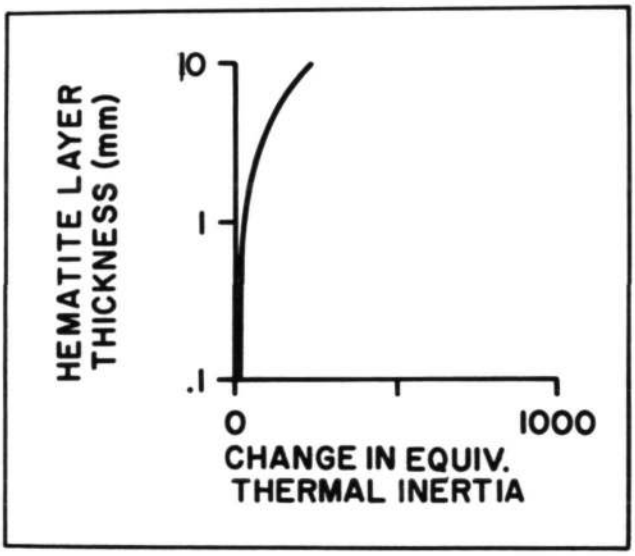

Figure 3.--Change in equivalent thermal inertia for a variable thickness hematite layer.

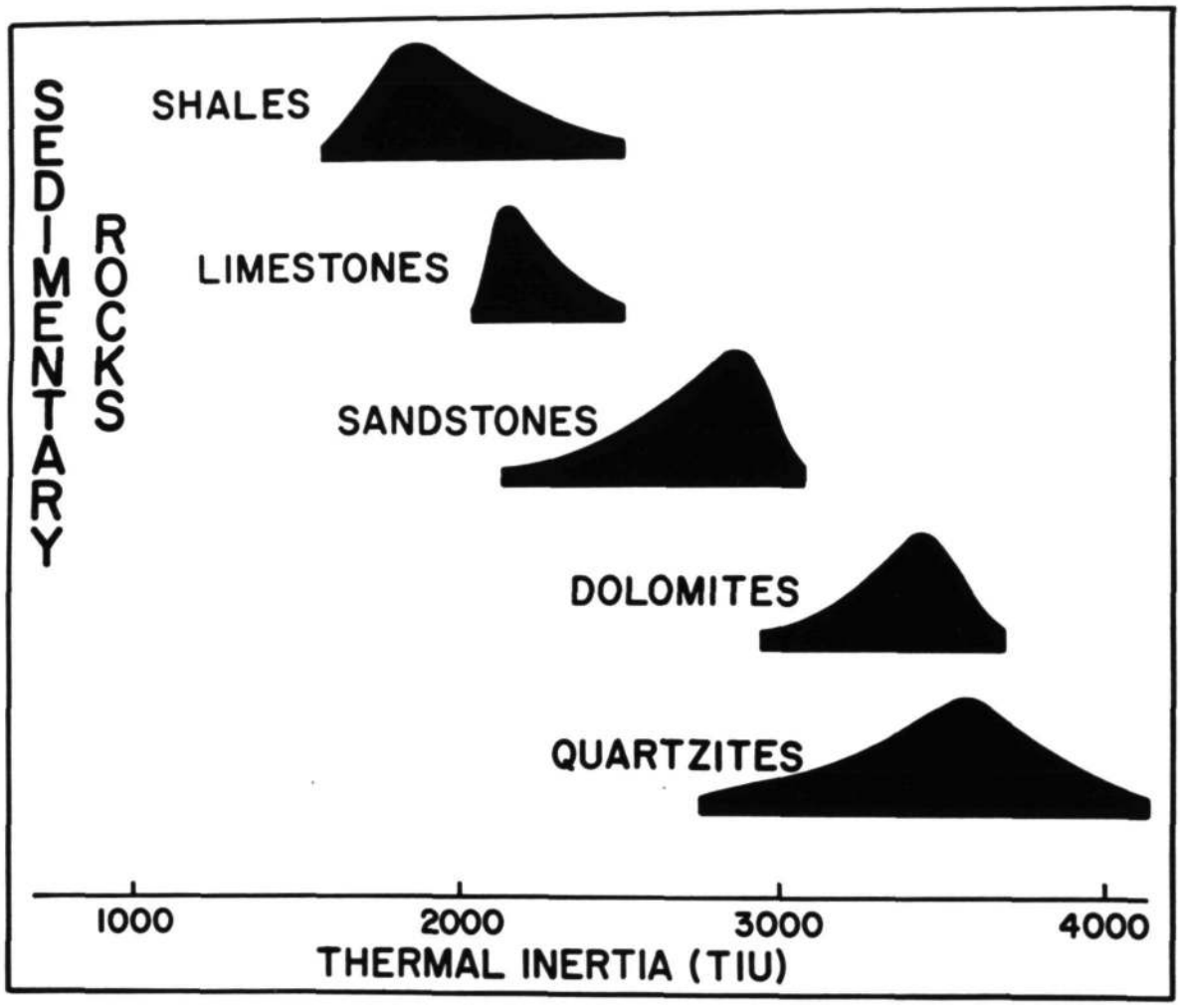

Figure 4.--Histograms of the range of thermal inertias for some sedimentary rocks [12], [13].

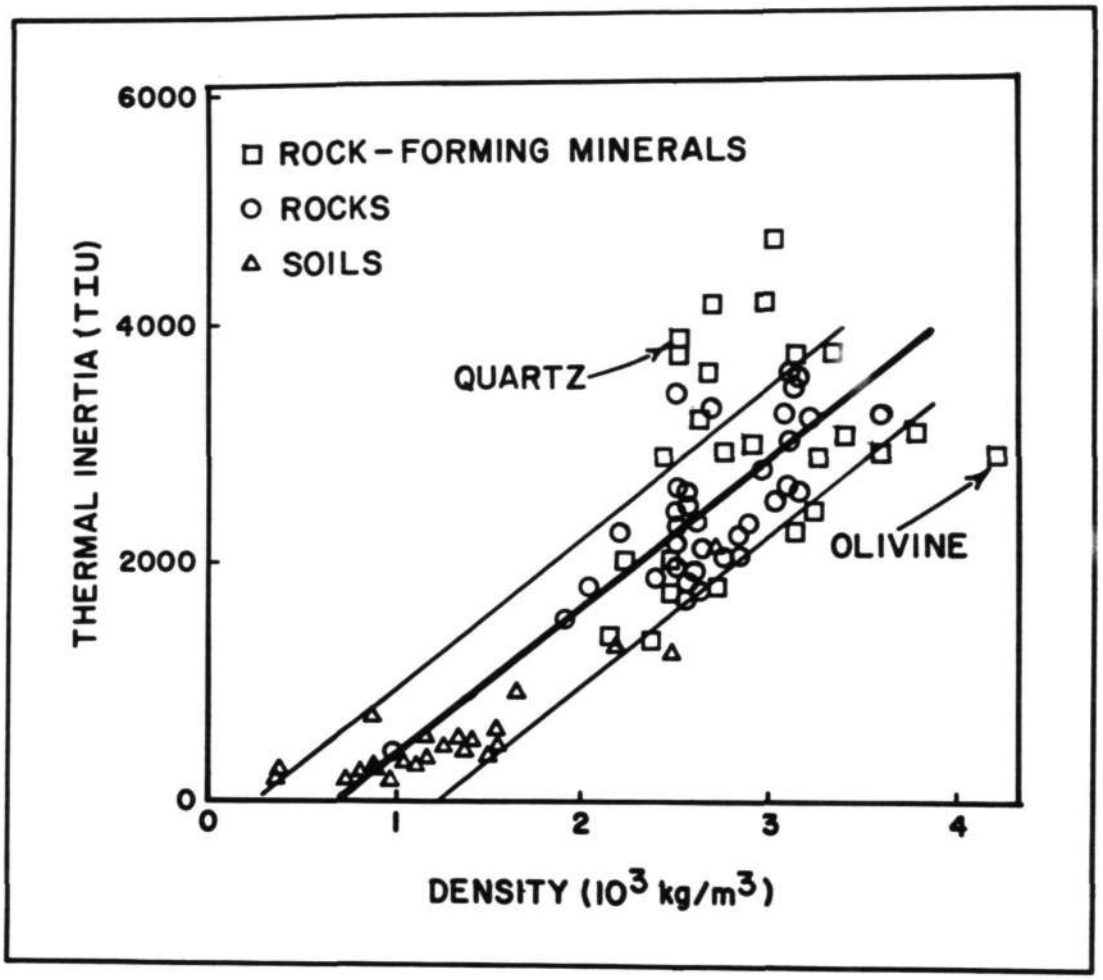

Figure 5.--Thermal inertia versus density for a variety of rock forming minerals, rocks, and soils.

Figure 6.--Thermal image acquired at 1430 hours of an area of the Raft River, Id., July 31, 1974.

Figure 7.--Thermal image acquired at 2300 hours of an area of the Raft River, Id., July 31, 1974.

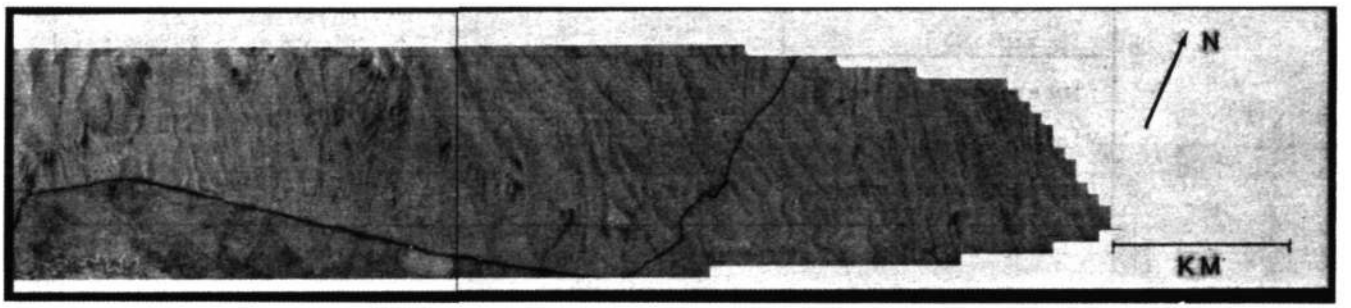

Figure 8.--Reflectance image acquired at 1430 hours of an area of the Raft Fiver, Id., July 31, 1974.

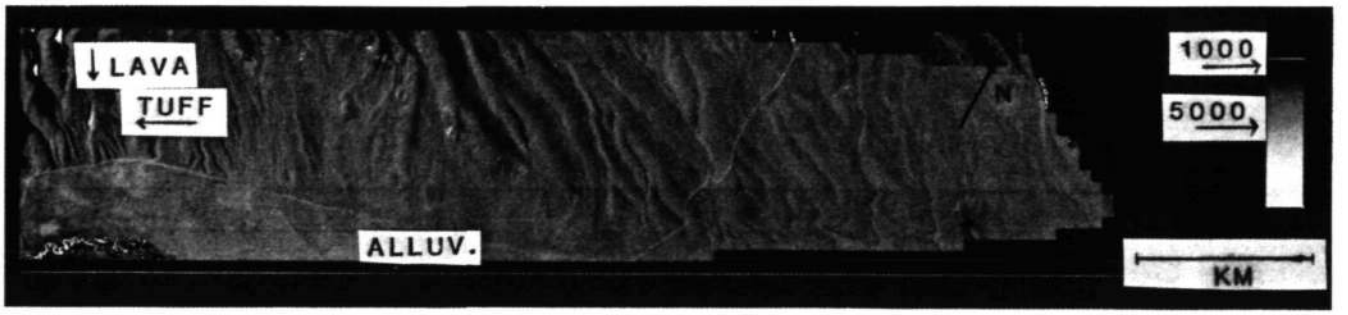

Figure 9.--Thermal-inertia map created from the 1430 and 2300 hours thermal image and a 1430 reflectance image of an area of the Raft River, Id.

TABLE 1. Parameter values used to compare the three algorithms.

F_0 = 475 watts/m^2
T_{sky} = 260°K
ε = 1.0
Δt = 8640 sec (0.1 day)
Δx = 0.12 m

TABLE 2. Relative ranking of algorithms with respect to cost/effectiveness.

ALGORITHM	CRITERIA		
	Accuracy	Computer Time	Visualizing Physical Significance of Parameters
Linear Fourier Series	Least	Least	Yes
Finite Difference	Median	Median	No
Laplace Transform	Most	Most	No

Table 3. Typical thermal-inertia values for a range of igneous rocks.

ROCK TYPE	THERMAL INERTIA (TIU)
Rhyolite	1950
Granite	2150
Basalt	2200
Gabbro	2350

Table 4. Typical thermal-inertia vlues for some geologic materials that were studied using Landsat data [9, 13].

ROCK TYPE	THERMAL INERTIA (TIU)
Black Shale	1900
Gabbro	2350
Basalt/Andesite	2200
Argillite	2250
Black Chert	3100